Lili: Liquor Quality Monitoring Based on Light Signals

Yongzhi Huang
huangyongzhi@email.szu.edu.cn
CSSE, Shenzhen University, Shenzhen, GD CN

Kaixin Chen
2017133035@email.szu.edu.cn
CSSE, Shenzhen University, Shenzhen, GD CN

Lu Wang
wanglu@szu.edu.cn
CSSE, Shenzhen University, Shenzhen, GD CN

Yinying Dong
1810272048@email.szu.edu.cn
CSSE, Shenzhen University, Shenzhen, GD CN

Qianyi Huang
huangqy@sustech.edu.cn
Institute of Future Networks, SUSTech, Shenzhen, GD CN

Kaishun Wu*
wu@szu.edu.cn
CSSE, Shenzhen University, Shenzhen, GD CN

ABSTRACT

In industrialized wine production, brewing and aging are two key steps. These two processes require the liquors to be bottled for a long time, sometimes more than ten years. The liquor is vulnerable and highly susceptible to microbial contamination during storage, causing undetectable deterioration. During the production process, wineries control the indoor temperature and carbon dioxide concentration to slow down other microorganisms' reproduction speed. These methods, however, do not prevent pathogenic microorganism growth. Currently, microbial culture methods are not suitable for real-time liquor quality monitoring in wineries. Therefore, we have designed a lightweight monitoring system called Lili, which uses light signals to monitor real-time liquor quality changes. Lili detects the changes in surface tension and absorption spectrum caused by microbial metabolites and growth during deterioration. Lili employs eight LEDs and one photodiode to achieve fine-grained surface tension and absorption spectrum measurements. By analyzing these changes, Lili realizes real-time quality monitoring. In this paper, the characteristic offset degree measurement and the absorption spectrum dimension expansion are two critical technologies. In addition, we implemented countermeasures against ambient light noise and sloshing interference. Lili's surface tension and absorption spectrum measurement errors are only 0.89 mN/m and 2.4%, respectively, making it useful to identify the contamination duration, microorganism content and microorganism composition. These two data points can be used to determine potential issues with liquor quality when the liquor becomes health-threatening or even just contaminated, with an accuracy of 97.5%.

*Kaishun Wu is the corresponding author

ACM MobiCom '21, October 25–29, 2021, New Orleans, LA, USA

ACM ISBN 978-1-4503-8342-4/21/10…$15.00
https://doi.org/10.1145/3447993.3483246

CCS CONCEPTS

• **Human-centered computing** → **Ubiquitous and mobile computing systems and tools**; • **Applied computing** → *Consumer health*; • **Computer systems organization** → Real-time systems.

KEYWORDS

Liquor quality; Long-term monitoring; Light signal; Absorption spectrum; Modeling; Fine-grained

ACM Reference Format:
Yongzhi Huang, Kaixin Chen, Lu Wang, Yinying Dong, Qianyi Huang, and Kaishun Wu. 2021. Lili: Liquor Quality Monitoring Based on Light Signals. In *The 27th Annual International Conference on Mobile Computing and Networking (ACM MobiCom '21), October 25–29, 2021, New Orleans, LA, USA.* ACM, New York, NY, USA, 13 pages. https://doi.org/10.1145/3447993.3483246

1 INTRODUCTION

In wine production [1], brewing and aging are two significant steps, lasting from several months to more than ten years, and can mask food safety risks. During this period, numerous microorganisms began to grow and multiply. The existing liquid quality measurement technologies, including the spread plate method with microbial cultures [2] and microbial detection based on ATP fluorescence [3], are tedious and expensive. To reduce costs [1, 4], specialized wineries control the wine cellar's temperature and carbon dioxide concentration to ensure that yeasts survive in a suitable environment. Such controls can reduce only the rate of pathogenic microorganism reproduction, and wine contamination cannot be detected until the end of aging by sampling and testing and can cause severe food safety issues in alcoholic beverages [5]. These deteriorating liquids are considered serious food safety hazards [6–8], causing fever, diarrhea, allergies, and even shock. For a long time, late detection of deteriorating liquids has resulted in severe economic losses in manufacturing [9, 10]. Deteriorated liquid contains pathogenic microorganisms [11, 12], including *Staphylococcus aureus*, *Escherichia coli*, *Vibrio casei, Halomonas*, *Aspergillus flavus, Salmonella, Penicillium, Mucor, Serratia*, *Aspergillus niger*, etc. These microorganisms produce a great number of harmful or even carcinogenic substances [13, 14], such as nitrite, aflatoxin, ammonia and hydrogen sulfide. According to a 2020 report from the World Health Organization [15]: 600 million – almost 1 in 10 people globally – fall ill after eating contaminated food, and 420,000 die every year, resulting in the loss of 33 million healthy life years (DALYs).

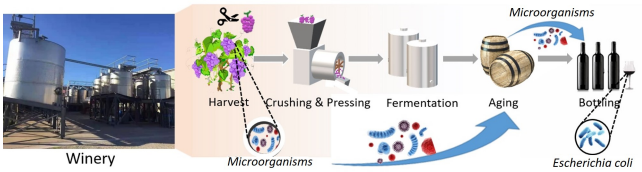

Figure 1: Winery and brewing process.

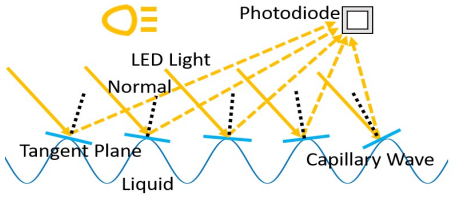

Figure 2: Cross section schematic diagram.

Safety testing in a winery involves two main sets of product tests: determining chemical indexes and microbial culture counts, including pH measurements [16], the spread plate method with microbial cultures [2], and microbial detection based on ATP fluorescence [3, 17]. Such testing is time-consuming and cumbersome and has a high probability of inspection misses. Some researchers have designed an electronic nose [18] to identify deterioration through smell fingerprints. This expensive high-precision equipment can detect deterioration only when barrels are open and cannot detect real-time deterioration during the production process. The latest studies have used different technologies, including detection based on light signals [19, 20], RFID [21], ultra-bandwidth signals [22] and mechanical vibrations [23] to identify liquids, but they are difficult to employ in the production process.

Against this backdrop, we pose some questions to address these challenges. Can we find an alternative to the traditional methods of microbial cultivation? Is it possible to achieve real-time liquor quality measurements, can they be made with common instrumentation? Researchers found that deterioration can change liquid properties [20, 24, 25], especially at the surface. Deterioration of a liquid will change its surface tension [24, 25], and the microorganisms inside will further cause a subtle change in the absorption spectrum [20]. The microorganisms on a liquid surface change the composition by decomposing the original nutrients and releasing metabolites. Therefore, if we can conduct the surface tension and absorption spectrum measurement within a short time interval, we can achieve real-time monitoring of liquor quality.

Although numerous studies have proposed measurement methods for the surface tension [26–28] and absorption spectrum [29–31] of liquids, the acquisition of traditional detection instruments, which are large and expensive, is difficult for many laboratories. In the latest research, researchers have continued to increase the accessibility and simplicity of surface tension detection methods [32, 33]. For example, CapCam [33] uses a mobile phone's high-definition camera to measure surface tension of a liquid through the bottom of a disposable paper cup, but it is challenging to measure nontransparent liquids, such as red wine, within a sealed container with this device.

In this paper, we propose a lightweight system named Lili—liquor quality monitoring with light signals—that can be installed in brewing equipment after encapsulation. Instead of using cameras or other expensive components, Lili utilizes only 8 LEDs and a single photodiode. Lili activates a vibro-motor on a container to generate capillary waves during measurement. From reflected light, Lili can perceive subtle alterations in surface tension caused by liquor deterioration. Using self-designed dimension expansion technology, Lili adjusts the LEDs to achieve fine-grained absorption spectrum measurements to identify tiny changes in liquor composition after vibration ceases.

There are several challenges to implementing this system. First, a single photodiode cannot capture capillary waves directly via imaging, so we need to establish a model to characterize capillary wave wavelengths. Second, affected by vibration disturbances, the received light signal produces many complex frequency signals, making it difficult for us to find the features resulting from the capillary wave wavelength changes. Third, as the LED waveband is narrow, the reflected light can display the absorption spectrum in only this narrow waveband. Moreover, this narrow-band reflected light compresses to an average value after being received by the photodiode. With this coarse-grained information, it is difficult to identify the subtle changes caused by microbial decomposition and metabolism. Fourth, reducing the effects of ambient interferences is challenging.

Contributions: We are the first to propose a real-time monitoring system, Lili, for liquor quality. Lili can be installed on brewing equipment for long-term monitoring. Furthermore, because it uses common instrumentation, Lili has low power consumption and is inexpensive and suitable for large-scale deployment. Moreover, we have proposed a new surface tension measurement with an error of only 0.89 mN/m. Finally, we designed a dimension expansion method for a coarse-grained absorption spectrum that detects very small changes in liquor components caused by decomposition of the original nutrients and metabolite release.

The rest of the paper is organized as follows: In Section 2, we detail how the LED and photodiode modules can detect the features of liquor surface tension and absorption spectra on the basis of theoretical models. Section 3 describes a feasibility study. After a system overview in Section 4, we introduce the system design and illustrate how we addressed the challenges in Section 5. In Section 6, we present several case studies evaluating the system performance. We discuss related work in Section 7 and conclusions and future work in Section 8.

2 THEORY OF OPERATIONS

This section will introduce the theoretical models for liquor quality detection.

2.1 Surface Tension

Surface tension is an essential property of liquids. Generally, liquid surface molecules will reduce the contact area with air to maintain the most negligible surface energy. The force among liquid surface molecules is called surface tension, a type of van der Waals force. Surface tension can be expressed as [34, 35], $\omega^2 = gK + \frac{\gamma K^3}{\rho}$. ω is the angular frequency of a surface capillary wave, K is the wavenumber of the surface capillary wave, γ is the surface tension, ρ is the

liquid density, and g is acceleration due to gravity. Pathogenic microorganism contamination causes liquid quality deterioration and produces harmful carcinogenic metabolites. These microorganisms need oxygen to multiply and therefore first grow on the surface of a liquid. The decomposed nutrients and released metabolites from growing microorganisms affect the van der Waals forces between molecules, consequently changing the surface tension. By analyzing these changes, we can monitor liquor quality.

2.2 Principle behind the Surface Tension Measurement

Considering cost and power consumption, we use the most common LEDs and photodiodes. In this section, we explain how LEDs and photodiodes can be used to measure surface tension. Because capillary waves are tiny and far away from the LED, we can assume that the incident rays that project to the liquid surface are parallel. As shown in Figure 2, due to the arc shape, each convex wave can exist in only one tangent plane that satisfies the law of reflection; that is, the angle of incidence is equal to the angle of reflection.

To find the reflection point locations, we model the reflective liquid. As shown in Figure 3, we assume that a surface capillary wave generated by a liquid is a sine curve, $y = \sin x$, and the point $(a_0, \sin a_0)$ on the curve is the reflection point. The receiver is a photodiode, which locates at the Cartesian axes (L, H). Then, we can obtain the tangent equation at this point as $y = \sin a_0 + \cos a_0\,(x - a_0)$. Next, we can get the reflection path equation: $y = \frac{\sin a_0 - H}{a_0 - L}x - \frac{(\sin a_0 - H)L}{a_0 - L} + H$. Because the normal line is perpendicular to the tangent plane, we can infer that the normal line equation is $y = \sin a_0 - \frac{1}{\cos a_0}\,(x - a_0)$. At this moment, we can use y to calculate the reflection angle between the reflected ray and the normal $\alpha_1 = \arctan\left|\frac{\frac{\sin a_0 - H}{a_0 - L} + \frac{1}{\cos a_0}}{1 - \frac{\sin a_0 - H}{a_0 - L}\frac{1}{\cos a_0}}\right|$. As the incident rays are parallel, we assume that the angle with the horizontal plane is β. Then, we can obtain the incident angle between the incident ray and the normal, $\alpha_2 = \arctan\left|\frac{\tan\beta + \frac{1}{\cos a_0}}{1 - \frac{\tan\beta}{\cos a_0}}\right|$. We simultaneously set α_1 and α_2, let $\alpha_1 = \alpha_2$, set $a_0 = k\lambda + c$, and then obtain all feasible solutions, which are the tangent plane positions of each convex wave. Among them, λ is the capillary wave wavelength, k is a nonnegative integer, $0 < c < \lambda$.

Next, we use the feasible solutions to establish a simulation model. As shown in Figure 4 (a), we set two different liquid surface tensions γ_1 and γ_2 ($\gamma_1 > \gamma_2$), and the wavelengths of the capillary waves are λ_1 and λ_2 ($\lambda_1 > \lambda_2$). Considering that there will be scattering in light propagation, we set the area around the reflection point as the photodiode's receiving range. When the vibration generates capillary waves, they spread from the center to the surroundings, and these ripples will spread outward at a constant velocity V. We assume that the area inside the rectangle is the photodiode's receiving area. After that, we calculate the total light intensity received by the photodiode and observe the change over time. As shown in Figure 4 (b), lower surface tension will result in a higher frequency of the reflected light signal.

2.3 Absorption Spectrum

In this section, we introduce how liquid composition changes affect the absorption spectrum. When electromagnetic waves irradiate a substance, phenomena such as transmission, absorption and scattering occur. These phenomena come from interactions between the electromagnetic waves and internal components (such as atoms, molecules and macromolecules), influencing the wavelength [36]. For example, in Figure 5, the energy of an atom is quantized, forming energy levels. When the atom is in a completely free state, it has the lowest energy, called the ground state energy E_0. Under the action of heat, electrical energy or light energy, the ground state absorbs energy. The outermost electron undergoes a transition from a low energy state to a higher energy state, resulting in an excited state atom. The wavelength and frequency of the atomic absorption spectrum are determined by the energy difference ΔE between the two energy levels that produce the transition: $\Delta E = E_q - E_0 = \frac{hc}{\lambda} = h\upsilon$. E_q is the energy of the excited atom, E_0 is the ground-state energy, λ is the wavelength in the spectrum, υ is the frequency, c is the speed of light, and h is the Planck constant. The ground-state atom can transition to the high-energy state E_q only by absorbing light with a frequency of $\upsilon = \frac{E_q - E_0}{h}$. Therefore, the atomic absorption spectral line also depends on the element's atomic structure, and each element has characteristic absorption lines. The number of spectral lines directly depends on the number of atomic energy levels. Suppose the number of atomic energy levels is n, and the ground state is excited to all levels of highly excited states. In that case, the number of atomic absorption spectra that may be generated is $N_{em} = \frac{n^2}{2}$.

Microorganisms change the liquid composition and destroy parts of an element's atomic structure, leading to changes in the element composition. Therefore, the interaction between light and the substance interior is also changed, which can be reflected in the absorption spectrum.

3 FEASIBILITY STUDY

We verify the proposed model and demonstrate its feasibility with a 3D-printed cup in this section

3.1 Experimental Setup

To verify the feasibility of the model, we used common plastic polymethylmethacrylate (PMMA) in this experiment to print a double-layered cup as the container, as shown in Figure 6. We installed a Taptic Engine Vibro-motor on the bottom of the inner cup as the driving force to generate capillary waves. The inner cup was 7.3 cm in diameter, 8.1 cm in height, and 1 mm in thickness and could hold 300 ml when vibrating. The outer cup was 4 mm larger in diameter than the inner cup. The double-layer structure allowed the outer cup to be separated from the inner cup, which protected the outer cup from vibration. On the top, there was a 2 mm thick flat plate as the lid and eleven alternately mounted LEDs with different wavelengths (940 nm, 1070 nm, 1200 nm, 1300 nm, 1370 nm, 1460 nm, 1550 nm, 1600 nm, 1700 nm, 1850 nm and 1950 nm) on one side 2 cm away from the circle center. The lid fit on the outer cup. An InGaAs photodiode has an acceptable spectral range of 800-2000 nm, with sampling at 5.6 kHz. We used a JK99B surface tension detector and NIR2500 spectrometer to measure the surface tension and absorption spectrum (900-2500 nm). We also used a Sysmex-Partec CyFlow Cube 6 flow cytometer (FCM) detector to determine the microbial counts. The following experiments were

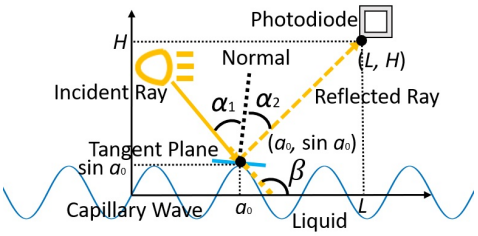

Figure 3: Model of the location of a reflection point.

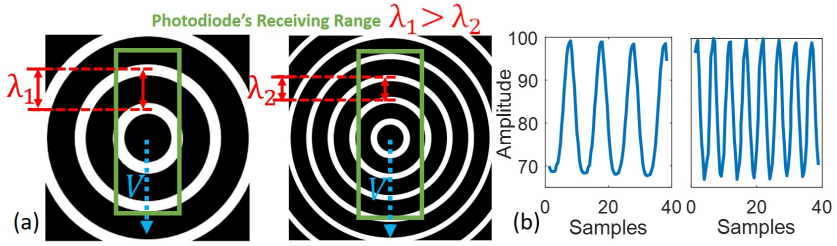

Figure 4: Simulation model. (a) Top view. (b) Changes in the intensity of light received by the photodiode.

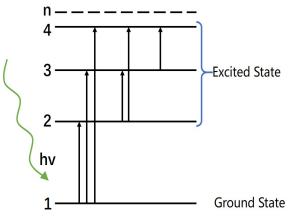

Figure 5: Absorption Spectrum Model.

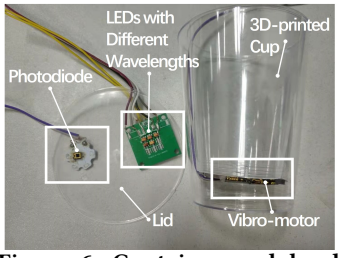

Figure 6: Container and hardware module for the confirmatory experiment.

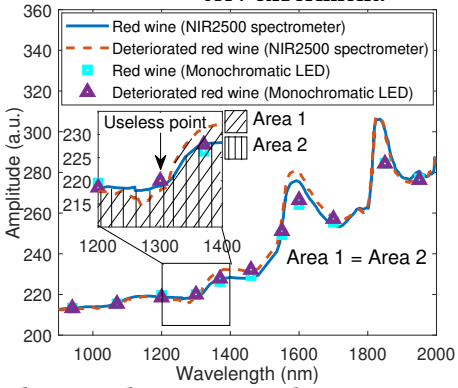

Figure 7: The monochromatic LED absorption spectrum and the ground-truth spectrum from the spectrometer.

performed in a dark room at 25℃. We conducted experiments on liquids during the aging of four types of wine: red wine (crushed grapes), rice wine (glutinous rice), sake (rice) and spirits (sorghum and corn).

3.2 Reflected Light Signal of Contaminated Liquor

We utilized brewed semifinished wine in these experiments and *E. coli*, a common pathogenic microorganism, as a contaminant. We dropped an *E. coli* culture solution (2.7×10^6 cells/ml) into the four semifinished wines and exposed them to air for 72 hours. The experiments mimicked the contamination of microorganisms during the aging process of wine. We prepared ten replicates of each sample. To prevent interference from vibration, we fixed the lid on a separate column. Moreover, we analyzed the surface tension, the reflected light signal (under vibrating and static conditions) and the absorption spectrum of the wine every 30 minutes. When vibration began, we turned on all the LED lights and adjusted the duty cycle to 100%. Next, we collected the reflected light signal from the photodiode for 5 seconds. Then, we converted the signal to the frequency domain and found the most significant peak frequency. As shown in Figure 8, we observed that the surface tension was negatively correlated with the peak frequency. This phenomenon was consistent with the simulation model in Section 2.2.

In the next step, we stopped the vibration and used the LED to irradiate the each liquid sample for 2 seconds. Subsequently, we analyzed the intensity of the reflected light received by the photodiode (arbitrary units) and arranged the values obtained by each LED in ascending order of light wave wavelength. The reorder vector was called the LED absorption spectrum. Furthermore, we used an NIR2500 spectrometer to measure the ground-truth absorption spectrum. As shown in Figure 7, the monochromatic LED absorption spectrum was not sensitive to liquid deterioration because the change in absorption spectrum was not uniform and some spectral regions did not change as the liquid deteriorated. As shown in the ground-truth spectra, as deterioration occurred, the absorption spectrum underwent the most significant changes near 1300 nm, 1400 nm, 1460 nm, 1600 nm and 1700 nm.

3.3 Measurement of Liquor Deterioration

To assess liquor deterioration, we measured the surface tension and absorption spectrum of the four uncontaminated wines after aging for 72 hours. The surface tension changes among the different wines were inconsistent, as shown in Figure 9 (a), because the raw materials were different. We also measured the surface tension changes in different samples of contaminated red wine. Figure 9 (b) shows that the surface tension of the contaminated samples fluctuated over time. However, the same surface tension can be recorded from both a deteriorated sample and an undeteriorated sample, prohibiting the determination of the deterioration degree. Therefore, this parameter must be combined with other characteristics, such as the absorption spectrum. In Figure 10, we show the changes in the absorption spectra of different wines during aging. The intensities near wavelengths of 1250 nm, 1400 nm, 1460 nm, 1600 nm and 1700 nm change significantly. This indicates that these wavelengths may be related to microorganisms and their metabolites.

Similar to the observations described in Section 3.2, the changes in the surface tension and absorption spectra of contaminated liquors are quite different from those of uncontaminated liquors. Considering these differences, we can use surface tension and the absorption spectrum together to assess liquor quality. However, unknown microorganisms may result in coincident eigenvectors at certain moments, which can make it difficult to establish evaluation criteria. Moreover, because it is impractical to determine

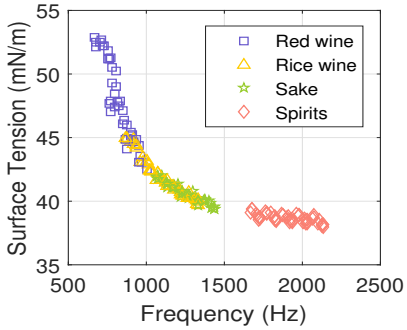

Figure 8: Variations in the surface tension and reflected signal peak frequency of different wines.

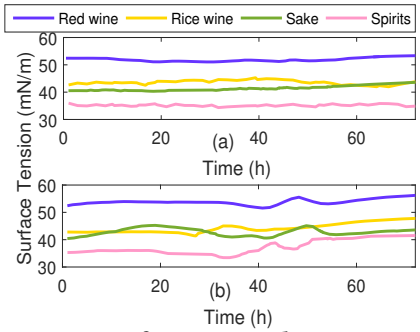

Figure 9: Surface tension during aging. (a) Uncontaminated wines. (b) Contaminated wines.

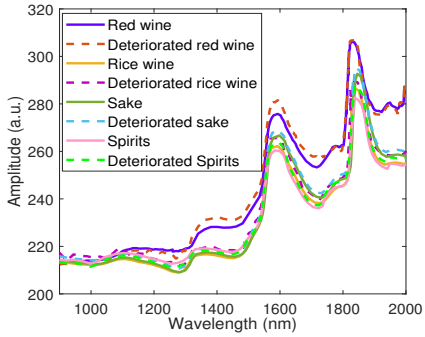

Figure 10: Absorption spectra of different wines during aging.

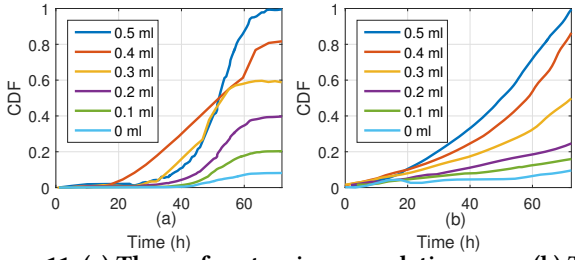

Figure 11: (a) The surface tension cumulative error. (b) The cumulative error in the absorption spectrum vectors.

all microorganism characteristics, feature classification cannot be used to evaluate liquor quality. To solve this problem, we propose a new discrimination method based on the feature path deviation degree that takes advantage of the temporal variation of features. The principle behind this method is to transform the eigenvector into a time-varying path in superdimensional space and calculate the degree of deviation between the measurement path and the standard path.

We first needed to normalize the uncontaminated liquor eigenvectors. We mapped every dimension to the interval $[0, 1]$ and obtained the standard $\vec{L}_{Ref} = [SF_t, AS_i(t)]$, where t is the time, SF is the surface tension value, and AS is the absorption spectrum vector. We set the initial point $\vec{L}_{Ref}(t_0) = \left[SF_{t_0}, AS_i(t_0)\right]$ as the reference point and calculated the difference between the measured point and the reference point at each moment $\Delta\vec{L}_{Ref}(t_0) = \vec{L}_{Ref}(t) - \vec{L}_{Ref}(t_0)$. We set the $end-1$ difference vector $\Delta\vec{L}_{Ref}(t_0)$ from t_0 to t_{end} as the standard path.

We used red wine as the experimental object and set up ten experimental groups. Each group received 1 - 10 drops (0.05 ml/drop) of *E. coli* culture solution (2.7×10^4 cells/ml) and was analyzed every half an hour over a 72-hour period. We used *E. coli*, which is generally used to assess sanitary conditions in food handling environments [37]. In general [37–39], an environment is considered very hygienic if the number of Enterobacteriaceae bacteria detected per gram of food is less than 10^2 units. If the number measured is more than 10^4 units, the food poses a health risk. Food in the middle range is unsanitary but does not affect health. In the experiments, the liquid volume was 300 ml. A drop of *E. coli* culture solution was equivalent to a 4.5 cells/ml increase in *E. coli* in the liquors. Liquors contaminated by microorganisms produce substances harmful, such as nitrite, in the body. The World Health Organization Joint Expert Committee on Food Additives (JECFA) stipulates that the daily allowable nitrite intake is 0-0.2 mg/kg·bw [40]. According to research data [41], health impacts occur after deterioration for 14 to 48 hours. If the deterioration time exceeds 72 hours, severe physical discomfort may result from ingesting the food.

We established two measurement tables containing the surface tension and the absorption spectrum data and calculated the contaminated experimental group's relative cumulative variance error based on the uncontaminated control group. Each microorganism has a unique absorption spectrum fingerprint [42, 43], and as they grow, the surface tension changes significantly [24, 25]. Therefore, we used the surface tension and absorption spectra to assess two categories, the contamination time and microorganism content. The contamination time was divided into 12-hour periods, labelled $I - VI$. The microorganism contents were divided into four levels: $Hygiene++$ ($0 - 10^2$ units), $Hygiene+$ ($10^2 - 10^3$ units), $Hygiene-$ ($10^3 - 10^4$ units), $Unhygienic$ (greater than 10^4 units). As shown in Figure 11, just after liquor contamination, the cumulative error in the surface tension was almost 0. However, the cumulative error in the absorption spectrum vectors increased significantly. Over time, the increase in the error as more drops of *E. coli* culture solution were added accelerated. We refer to these cumulative errors as the feature path deviation degree. Using the measurement tables, we determined the degree of liquor deterioration according to the feature deviation. When aging began, we recorded every measurement vector $\vec{L}_{Mea}(t) = [MSF_t, MAS_i(t)]$ and calculated the difference between the measurement vector and the initial point $\vec{L}_{Mea}(t_0) = \left[MSF_{t_0}, MAS_i(t_0)\right]$ to obtain the measurement path $\Delta\vec{L}_{Mea}(t_0)$. By comparing the same time point with the standard path, we calculated the feature path deviation degree to determine the liquor deterioration degree from the measurement tables.

4 SYSTEM OVERVIEW

Lili is composed of five modules, as shown in Figure 12.

Signal Drive Module: This module controls the motor vibration, drives the LEDs, adjusts the light intensity, and simultaneously collects the light signal received by the photodiode.

Environmental Interference Reduction Module: Two kinds of interference are encountered: ambient light noise and external vibration interference. During monitoring, if the container is not entirely opaque or closed, ambient light noise may be introduced.

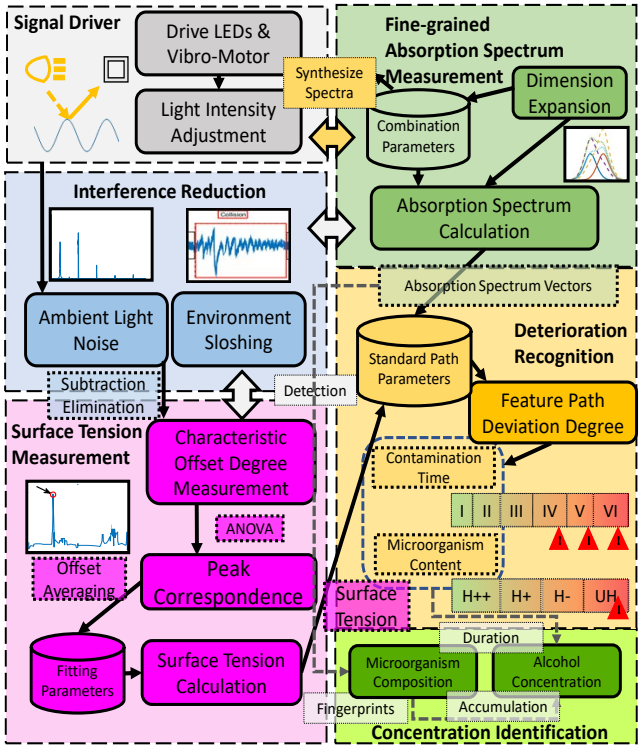

Figure 12: The workflow of Lili.

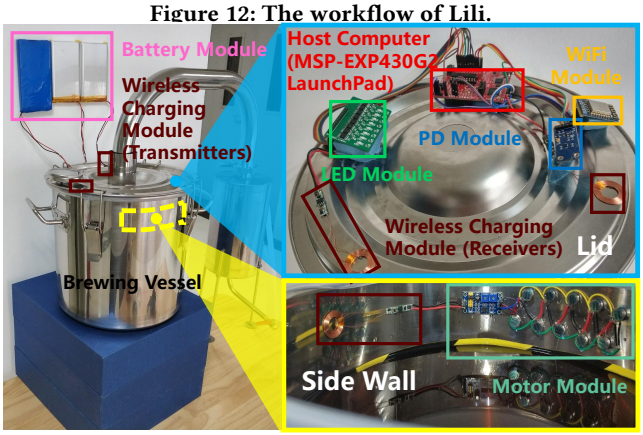

Figure 13: Deployment of Lili prototype on brewing vessel.

Similar to the vibration used to generate capillary waves, external vibration (for example, knocks and footsteps) will cause severe interference with the detection. This module reduces the impacts of these interferences on detection.

Surface Tension Measurement Module: This module analyzes the collected light signal and records the current surface tension. Then, the change in surface tension relative to the standard signal from the original undeteriorated liquor is determined.

Absorption Spectrum Analysis Module: This module controls the signal drive module to perform fine-grained absorption spectrum analysis; spectra are compared with the absorption spectrum of the original liquor, and the variance is determined.

Deterioration Recognition Module: On the basis of the surface tension data and absorption spectrum data analyzed for the monitored liquor, this module identifies the degree of deterioration according to the type of liquor monitored.

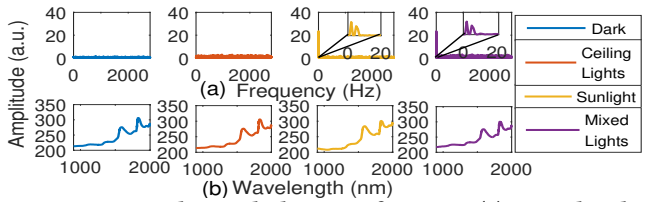

Figure 14: Ambient light interference. (a) Amplitude-frequency diagram for the photodiode. (b) The environmental spectrum of the spectrometer.

5 SYSTEM DESIGN OF LILI

5.1 Experimental Setup

In the Section 3, we presented the absorption spectra of four wines in two states, undeteriorated and deteriorated, during the aging process. We found that the peaks at wavelengths of 1300 nm, 1400 nm, 1460 nm, 1600 nm and 1700 nm differed the most significantly between the two states. Therefore, we used LEDs emitting at 1070 nm, 1200 nm, 1300 nm, 1460 nm, 1600 nm, 1700 nm, 1800 nm and 1900 nm to cover the peak wavelengths and an InGaAs photodiode, which has an acceptable spectral range of 800-2000 nm. We welded the LEDs and photodiode to two self-designed circuit boards. As shown in Figure 13, a Texas Instruments MSP-EXP430G2 LaunchPad was the host computer, and the sampling rate was set to 5.6 kHz. The host computer was connected to an ATK-ESP8266 WiFi module to ensure data transmission. The host computer controls the LED module through a pulse width modulator (PWM) connected to GP8101. GP8101 can convert 0-100% duty cycle PWM signals into 0-5 V voltage signals. We designed a spare part, a wireless charging module beside the battery module, which can emit 5 V/500 mA. We installed the host computer, LED module, photodiode module, WiFi module, battery module and wireless charging module on the brewing equipment's lid. Ten B1036F1 vertical linear motors were installed on the brewing vessel wall to generate capillary waves, which were controlled through the NE555 pulse generator. They are all covered with a layer of waterproof nanospray. We tested the system with different materials in small industrial brewing equipment at room temperature ($25^{\circ}C$), including stainless steel, wood, glass and ceramics, and volumes of 12 L, 22 L, 36 L and 50 L. Simultaneously, we used a JK99B surface tension detector, an NIR2500 absorption spectrometer, and a Sysmex-Partec CyFlow Cube 6 flow cytometer (FCM) to measure the ground-truth data, and the cost of each was approximately \$5,000, \$15,000, \$8,000, respectively.

5.2 Interference Elimination

5.2.1 Eliminate Ambient light Noise. Some manufacturers use light-transmitting materials (such as glass) as containers or light-transmitting lids for easy observation during the aging process. These containers may allow ambient light radiation to reach the photodiode. Noise from ambient light may come from sunlight and surrounding lights (such as lightbulbs). Therefore, we used Lili's photodiode and spectrometer to collect data in three different experimental environments: an office, a conference room and a laboratory. The ceiling lights were T8 fluorescent lights. We recorded the light signals under four conditions: dark, sunlight, ceiling lights, and mixed lights.

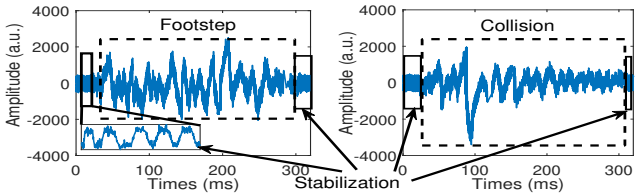

Figure 15: Interference from footsteps and collisions from people nearby on the time-domain signals

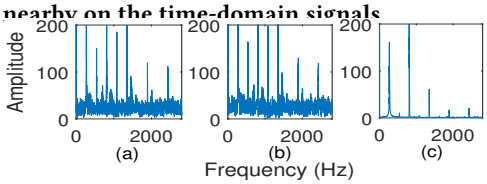

Figure 16: (a) & (b) Different surface tension signals during vibration. (c) Signal when the lid was fixed.

As shown in Figure 14, the photodiode signal was only slightly noisy in the dark and ceiling light scenarios, and the spectrum remained flat at a low amplitude. When the ambient light was sunlight, the photodiode detected low-frequency noise with a relatively high amplitude, and the spectrum fluctuated. Although the noise was relatively low in all scenarios, these environmental interferences need to be eliminated to reduce errors. Therefore, before detection, Lili turns off the LEDs and calculates the ambient light's average amplitude-frequency curve. After Lili enters the test mode, it subtracts the ambient light amplitude-frequency curve from the signal.

5.2.2 Reducing Interference from Sloshing. The steps and collisions of people near a container will cause the liquor to slosh, which will affect the measurements. This sloshing comes from the inertial motion generated by an external force acting on the liquid, which is different from the motion of liquid capillary waves. This force disrupts the equilibrium in the liquid surface tension and interferes with capillary wave generation. Therefore, this interference will affect the accuracy of the measurement.

The footsteps and collision interference received by Lili's photodiode are depicted in Figure 15. These interferences caused significant long-lasting amplitude changes because inertial motion creates large specular reflection on the surface of the liquid. By analyzing the capillary wave reflected light signal, we discovered a stable period T, in which the sum of the amplitudes during that period remained constant. We determined that T lasted approximately 2 ms. We calculated the average amplitude $\bar{A} = \frac{1}{T}\sum_{t=0}^{T} I_t$. Then, we searched for a significant long-lasting amplitude change. After setting the period average as the dividing line, we calculated the amplitude and $S = \sum_{t=(n-1)T}^{nT} \left|I_t - \bar{A}\right|, n \in \mathbb{Z}^+$ within the period. By setting the threshold δ for the sum of the amplitudes S, we determined whether sloshing interference occurred. By suspending the measurement for 30 s, we avoided this interference.

5.3 Surface Tension Calculation

5.3.1 Challenge. In Section 2, we introduced how LEDs can measure surface tension by reflecting capillary waves, and the model was verified in Section 3. However, when we applied the system to brewing equipment, we encountered a challenge. As shown in Figure 16 (a), the LED reflected light signal had tremendous noise, making it difficult to directly observe the frequency offset even when the surface tension increased, as shown in Figure 16 (b). Since the brewing equipment was not double-layered like the 3D-printed cup in Section 3, vibration from the container wall affected the lid even if it was fixed to a separate column. Therefore, the LED and photodiode modules interfered with the vibration and produced considerable noise when the motor generated the capillary waves. However, traditional filters are not suitable for this complex frequency noise elimination because the masked feature seems to be noise and would be filtered out.

5.3.2 Observation. With complex frequency noise in the signal, the original frequency offset was challenging to find. We experimented with four types of wine, with 15 samples of each type (10 with different surface tensions + 5 with the same surface tension). We collected each sample for 10 seconds. A characteristic can be separated if its distribution is distinct from that of the noise. Therefore, we used 1 second as the window to observe the signal fluctuation law in the frequency domain among all samples. We calculated the variance for all frequency points. For convenience in expression, the variance for the same sample, the samples with the same surface tension, and the samples in different surface tension groups were named self-variance distribution, intragroup variance distribution and intergroup cross-variance distribution.

The self-variance distribution and the intragroup variance distribution had almost the same frequency point variance distribution. These distributions were relatively similar even if the surface tension was different. However, there were considerable differences in the intergroup cross-variance distribution. The observations show that the signal difference came from the change in surface tension related to the capillary wave reflection signal. Therefore, these reflections can be decomposed into the noise caused by vibration and the characteristics of capillary wave reflection.

5.3.3 Measurement of the Characteristic Offset Degree. This section introduces the method of finding the frequency offset. Figure 17 shows the simplified solution. The characteristic frequency offset is superimposed with the vibration noise because of the independence of the noise from the characteristic frequency. It is unrealistic to find the characteristic offset directly from the superimposed signal. However, if we calculate the absolute value of the difference between the two signal frequency curves, we obtain two apparent peaks in the frequency domain. Moreover, the distance between these two peaks is the characteristic frequency offset.

We regard the disturbance caused by white noise as the standardized normal distribution e_{tij}. The surface tension of a liquor in its initial state was used as the reference, so we consider the reference amplitude at each frequency point as $A_{t_0ij} = a_{t_0ij} + e_{t_0ij}$. A_{t_0ij} is the amplitude at frequency point j during the sequence i measurement at time t. a_{t_0ij} is the theoretical value for the initial state $t = t_0$, and e_{t_0ij} is the white noise of the normal distribution. Because the frequency offset causes more amplitude changes than the noise, we can divide the signal into three parts, $A_{tij} = a_{t_0j} + a_{tj} + e_{tij}$. Among them, a_{tj} is the disturbance caused by the measurement. In the detection, if a_{tj} can be regarded as 0, we believe that this frequency point does not have frequency offset characteristics. Therefore, we used analysis of variance (ANOVA) to infer this point, assuming

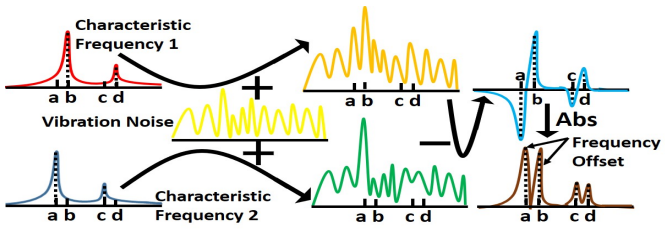

Figure 17: The solution of the characteristic offset.

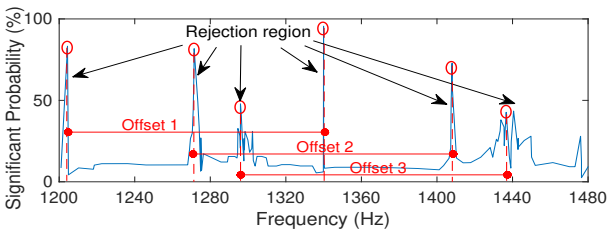

Figure 18: Frequency offset points found by ANOVA.

that a_{tj} can be regarded as 0. Each time, we collected ten samples and put them into the same group to calculate the random error at each frequency point.

To explain this clearly, we assume that ten samples are taken at time T, and each sampling lasts for 10 seconds. At this time, the random error of the frequency point can be expressed as $SS_e = \sum_t \sum_{i=1}^{10} \left(A_{tij} - \bar{A}_{ij}\right)^2, t = t_0, T$. Next, we compare with the liquor at $t = t_0$ to calculate the global deviation $SS = \sum_t \sum_{i=1}^{10} \left(A_{tij} - \bar{A}_j\right)^2, t = t_0, T$. The sum of the squares of the difference between the signal levels at time T is $SS_T = SS - SS_e$. We substitute the degrees of freedom and get $MS_T = \frac{SS_T}{k-1}, MS_e = \frac{SS_e}{n-k}$. We need to use the F-test to determine whether to accept the null hypothesis $\frac{MS_A}{MS_e} \leq F(\alpha)$.

As shown in Figure 18, we found offset frequency points between two samples with different surface tensions. The figure shows that there is more than one characteristic point, which is a result of the reflected light having different multipaths. Moreover, each peak representing the characteristic has another peak with a similar curve profile. This similar curve comes from the offset of the characteristic frequency. Therefore, we need to calculate the frequency difference between these corresponding characteristics.

To reduce the computational complexity, we used these two characteristics to find the frequency offset: the corresponding characteristic has a similar peak curve, and the frequency offset generated by any characteristic is approximate. We considered the peak point spacing within the threshold τ s the same peak curve and selected the peak at the median to represent the peak curve. Assuming that there are n peaks, we calculated the peak difference and frequency offset between all the peaks to obtain a matrix with a diagonal of

$$0, \begin{bmatrix} \left(\Delta_0^0 A, \Delta_0^0 F\right) & \cdots & \left(\Delta_0^{n-1} A, \Delta_0^{n-1} F\right) \\ \vdots & \ddots & \vdots \\ \left(\Delta_{n-1}^0 A, \Delta_{n-1}^0 F\right) & \cdots & \left(\Delta_{n-1}^{n-1} A, \Delta_{n-1}^{n-1} F\right) \end{bmatrix}.$$

We first selected the element $\Delta_0^i A$ in the first row from the non-diagonal elements and occupy column i. Then, $\Delta_0^i F$ was taken as the reference frequency offset. After that, we selected the non-diagonal element in other rows with three principles: ΔA was close to 0, the difference between ΔF and $\Delta_0^i F$ was close to 0, and the column was not occupied. After finishing the selection, we calculated all the selected element frequency offset variances $V_{\Delta F}$. Moreover, after traversing all elements in the first row, we chose the combination with the minimum variance $V_{\Delta F}(i) = \min\{V_{\Delta F}(m) | m \in [0, n-1]\}$. We averaged the frequency offset of all elements $\left\{\Delta_j^k F | (j,k) \in V_{\Delta F}(i)\right\}$ and then obtained the characteristic offset.

To verify the effectiveness, we expanded the method to other liquor experiments. We selected four kinds of liquors in Section 5.1 and calculated the average of the offset frequency point interval under 40 surface tension states. We analyzed the correlation between the value and the change in surface tension and calculated the Pearson correlation coefficient. The average Pearson correlation coefficient for the four liquors was greater than 0.9, indicating a significant correlation. To accurately calculate the change in surface tension, we established the corresponding relationship between the characteristic offset and the ground-truth surface tension change and used the least squares method to obtain the fitting function. In Section 3.3, we revealed that only the surface tension change needs to be monitored to assess the degree of liquor deterioration. However, to determine the real surface tension, the initial surface tension can be added to the surface tension change calculated from the fitting function.

5.4 Fine-Grained Absorption Spectrum Measurement

5.4.1 Limitations of the LEDs. Although the surface tension change can be used to identify liquor deterioration, some liquors may have the same surface tension even at different degrees of deterioration. Considering that deterioration involves the decomposition of the liquor and metabolite production by microorganisms, the material composition changes. From Section 2.3, which introduced the physical model of the absorption spectrum, we know that the absorption spectrum differs on the basis of these changes in material composition.

However, the metabolite alterations made by microorganisms are subtle. Lili is composed of only LEDs, so achieving measuring a fine-grained absorption spectrum is challenging, as LEDs can provide only a narrowband spectrum optical signal. When the detected object absorbs part of the light spectrum, we will obtain only an intensity value through the photodiode. The difference between this light intensity and the intensity of the light emitted from the original LED results in a coarse-grained absorption spectrum. However, within this waveband range, as long as the absorption spectrum area does not change, the coarse-grained absorption spectrum will not differ. Because of subtle changes in the absorption spectrum coupled with the noise from the system components, obtaining the same absorption spectrum area for different materials is common. Therefore, limited by the LED narrowband spectrum, it is difficult to detect subtle changes in the absorption spectrum with the photodiode.

5.4.2 Observation. To detect a fine-grained absorption spectrum with traditional methods, the emission waveband must be narrow, the band must be higher than what is traditional used, and a larger

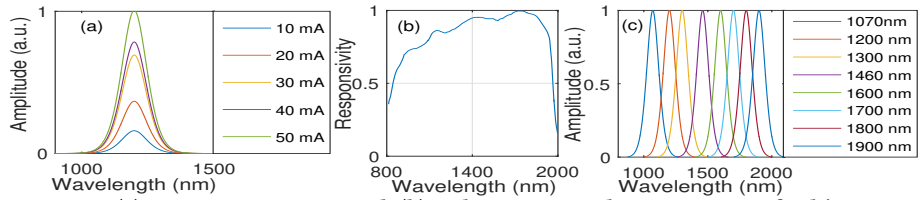

Figure 19: (a) LED spectrum expand. (b) Relative spectral responsivity of Lili's photodiode. (c) The spectral distribution of Lili's LEDs.

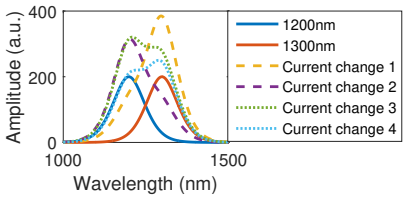

Figure 20: Spectrum synthesized example.

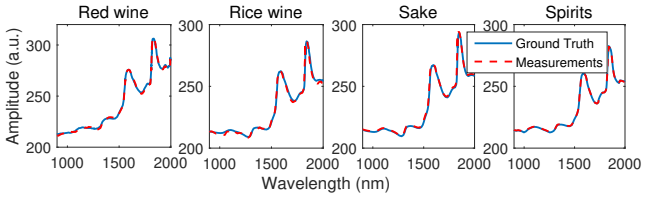

Figure 21: The absorption spectrum calculated from LEDs.

spectral range must be observed. In short, the resolution must be increased. There are two methods to achieve this goal: use expensive dispersive elements and sophisticated detectors such as spectrometers or use more light sources with different wavelengths and extremely narrow bands (such as lasers). However, these methods are expensive. If the reflected spectrum can be displayed in different dimensions, we can reduce the interference with the same absorption spectrum area and achieve a fine-grained inspection.

We first analyze the LED. The spectral radiation distribution of the LED is not a strictly symmetrical Gaussian distribution [44]. The peak wavelength's left end fits a Gaussian distribution function, and the right end fits a piecewise function of the Lorentz distribution function. Therefore, the LED spectrum can be simplified as $I(\lambda) = \alpha I_0 \times \exp\left[c_1\left(\frac{\lambda-\lambda_0}{\Delta\lambda}\right)^2 \times \exp\left(c_2\left|\frac{\lambda-\lambda_0}{\Delta\lambda}\right|\right)\right]$. $I(\lambda)$ is the intensity of radiation from an LED in the optical axis direction, λ is the incident wavelength, α is the current conversion coefficient, I_0 is the drive current, λ_0 is the centre wavelength, $\Delta\lambda$ is the full width at half maximum (FWHM), and c_1 and c_2 are constants.

From measurements, we found that the FWHM of the LED spectrum was not constant. As shown in Figure 19 (a), the original FWHM was 90 nm. Then, the drive current was increased from the original 10 mA to 50 mA while maintaining the operating voltage at 5 V. As the current increased, the FWHM of the LED spectrum gradually expanded. Therefore, wavebands beyond the original LED waveband can be covered by increasing the current.

5.4.3 Dimension Expansion of a Coarse-Grained Absorption Spectrum. In this section, we introduce how to expand the dimensions of a coarse-grained absorption spectrum. In brief, if the lights used to analyze a liquor have different spectral profiles, then subtle changes in the absorption spectrum will result in a different reflectance spectrum. Therefore, lights with different spectral profiles represent different dimensions of information. However, to measure these profile changes, we also need to consider the photodiode characteristics. Due to the photoelectric effect, light of different wavelengths can excite different photons in the PN junction and generate varying numbers of electrons. Therefore, the photodiode sensitivity changes. Figure 19 (b) presents a curve of the relative spectral responsivity of Lili's photodiode. We took advantage of the various responsivities of photodiodes to different light wavelengths and combined LEDs to achieve a signal sensitive to subtle changes in the absorption spectrum. Considering the LED waveband scalability presented in Section 5.4.2, we can superpose two different waveband spectra to obtain different spectral profiles for the lights. Moreover, adjusting the current leads to many available combinations, and these spectra will have a different center wavelength from the LED's original.

Therefore, the LEDs should have several characteristics. First, the wavebands of all LEDs should overlap with the detection frequency. Second, each LED spectral waveband should overlap with the others. Therefore, we selected eight LEDs with different wavelengths, as shown in Figure 19 (c). Because of their different internal structures, they had diverse luminous intensities and FWHMs.

Next, we introduce the method of generating the narrowband spectrum. Because the photodiode's ability to generate photons is limited, it will become saturated if the spectrum exceeds the threshold. At this time, regardless of the absorption spectrum changes, the current received will remain stable. Therefore, the emitted light intensity needs to be within the receiving range, which is the first constraint. To be conservative, we set the total light intensity of the synthesized spectrum to be less than or equal to the photodiode's receiving threshold.

In addition, we need to consider the different reflective properties of each liquor. Therefore, we need to detect the reflection coefficient of the liquor first. We started each LED at the maximum allowed current and reduced it until the photodiode value began to change. Then, we stopped decreasing the current and recorded the value $MaxI_\lambda$ as the maximum detection current for the given LED. Taking into account the rationality of the setting, we also need to remove useless amplification. If all LEDs of the same wavelength have the same amplification factor ratio for any two combinations of LEDs, then these two combinations are essentially the same, and one of them can be eliminated. Therefore, $TI_n = \sum_i \left[L_i(\lambda, {}^nk_\lambda) - PL - AS_\lambda\right] \cdot R_\lambda$, and we can determine all the constraints:

$$s.t. \begin{cases} TI_n \le Threshold_{PD} \\ {}^nk_\lambda I_\lambda \le MaxI_\lambda \\ \forall \{{}^nk_\lambda\} \ne \alpha \{{}^mk_\lambda\}, m \ne n, \alpha \in \mathbb{R}^+ \end{cases} \quad (1)$$

TI_n represents the total light intensity of the nth combination in the photodiode, which is the reflected light intensity multiplied by the responsivity R_λ. The reflected light intensity combines the LED light intensity $L_i(\lambda, {}^nk_\lambda)$, path loss PL , and absorption spectrum AS_λ. Each LED current may enlarge k_λ times the working current I_λ but should be less than or equal to the maximum current $MaxI_\lambda$. α is a positive real number. We set k_λ's step size to be 0.05 to calculate all the combination sets of k_λ for any two LEDs with overlapping

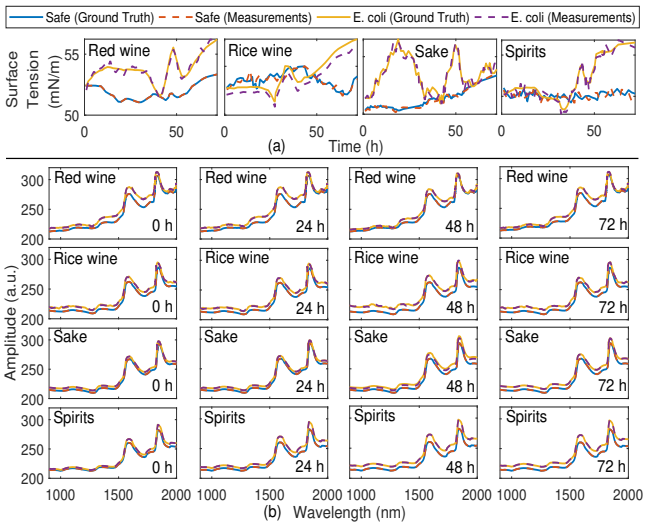

Figure 22: (a) Surface tension and (b) absorption spectra of different liquors measured by Lili.

wavelengths. Figure 20 shows some of the narrowband spectra produced by two LEDs with overlapping wavelengths.

After determining the combination of LED current values, we formulated each LED power sequence and current change. Then, we used a photodiode to record each reflected light value, thereby obtaining the dimensional expansion of the coarse-grained absorption spectrum. We substituted all the known values into TI_n and simultaneously $I(\lambda)$, used the Gaussian elimination method, built an augmented matrix, and solved the matrix with elementary row transformation. By solving the determinant, we obtained accurate absorption spectrum values. As shown in Figure 21, we compared the absorption spectra calculated from LEDs with the ground truth, and the mean absolute percentage error (MAPE) was only 0.7%.

6 SYSTEM EVALUATION

6.1 Liquor Monitoring Performance

6.1.1 Measurement Accuracy for Different Liquors. To verify Lili's performance in liquor monitoring, Lili monitored the aging process of different wines (red wine, rice wine, sake and spirits) for 72 hours. We divided the experiment into two groups: a normal aging group (the safety group), and a group contaminated with *E. coli* culture solution before aging (*E. coli* group). Before starting, we poured the wines into containers and maintained 25 cm between the liquid surface and the monitoring module. After measuring the initial surface tension and absorption spectrum, we input the data into Lili's database and began monitoring. The surface tension and absorption spectrum curves measured by Lili in Figure 22 are very close to the ground-truth data. The surface tension of the safety group changed relatively smoothly, unlike that of the *E. coli* group, which fluctuated widely. The absorption spectra of these two groups contained large fluctuations but were all concentrated on different wavebands. For the 72-hour monitoring period, the mean error in the liquid surface tension in the safety group was only 0.89 mN/m, while the mean error for the *E. coli* group was 1.16 mN/m. The mean absolute percentage error (MAPE) of the absorption spectra of the safety group and *E. coli* group was 2.37% and 3.04%, respectively.

6.1.2 Measurement Accuracy for Different Pathogenic Bacteria. In order to verify the monitoring ability of Lili for different pathogenic bacteria, we replaced *E. coli* with Salmonella and Staphylococcus aureus under the same experimental conditions as in Section 6.1.1. We calculated the mean error of surface tension and MAPE of absorption spectrum during the 72-hour monitoring. As shown in Figure 23, Lili can accurately monitor *Salmonella* and *Staphylococcus aureus (S. aureus)* contamination with very low error.

6.1.3 Measurement Accuracy with Different Container Volumes. The results for different container volumes are shown in Figure 24, as the volume increased, the surface tension error first decreased and then increased again. Initially, the interference caused by vibration decreased. However, as the volume increased, the container thickness also dramatically increased, and the capillary wave generated by the vibro-motor vibration decreased, which increased the interference caused by noise. The surface tension errors with the four container volumes were 0.89, 0.71, 0.65 and 1.24 mN/m while the MAPE of absorption spectra did not obviously change: 2.31%, 2.40%, 2.36% and 2.47%, respectively.

6.1.4 Measurement Accuracy with Different Container Materials. Considering that different merchants will use different container materials, we tested four container materials (stainless steel, wood, glass and ceramics) for spirits aging. Of the four types of containers shown in Figure 25, wood resulted in the worst performance, as the rigidity of wood materials is low and absorbs vibration energy. The low energy transmission causes the liquid capillary wave to decay quickly, which leads to significant measurement errors.

6.2 Liquors Quality Determination

6.2.1 Baseline. In Section 3.3, we set up two criteria for liquor quality based on the number of microorganisms and contents of metabolites that affect human health: the duration of contamination and the microorganism content. We took 40 samples of each of the four types of wine. The results shown in Figure 26 reflect a mean recognition accuracy rate of 95.1%. The accuracy of identifying categories that impact health (greater than IV, $Unhygienic$) was 97.5%. This means that Lili can accurately identify the deterioration of a liquor and prevent food safety accidents.

6.2.2 Ambient light Interference. We utilized glass containers to observe the quality assessment accuracy under four ambient light scenarios: dark, sunlight, ceiling lights, and mixed lights. The experimental results in Figure 27 show that Lili could adapt to different types of ambient light with a mean accuracy of 94.6%.

6.2.3 Interference from Liquor Sloshing. We created sloshing interference when Lili was running to observe the ability to reduce such interferences. The interference was generated by walking, dropping heavy objects, stomping, hitting the brewing vessel and moving the brewing vessel. As shown in Figure 28, Lili was very robust and could quickly distinguish sloshing interferences with a mean accuracy of 90.5%, and the mean response time was 7.8 ms.

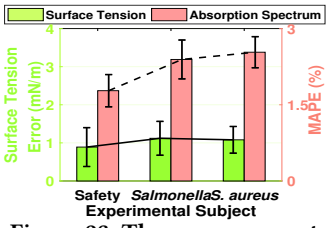

Figure 23: The measurement results for different pathogenic bacteria.

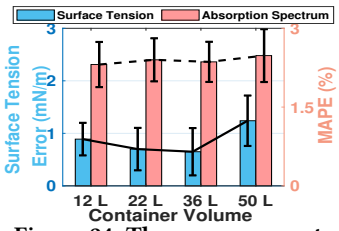

Figure 24: The measurement results for different container volumes.

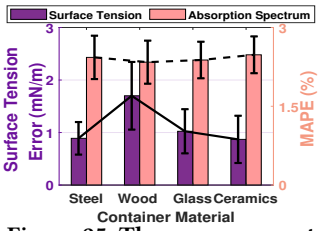

Figure 25: The measurement results for different container materials.

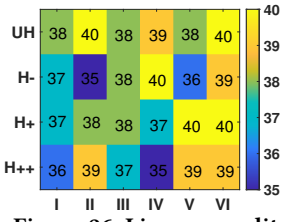

Figure 26: Liquors quality determination.

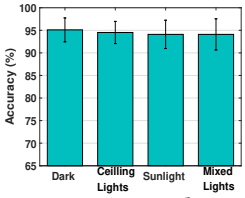

Figure 27: Quality assessment under different ambient light noise.

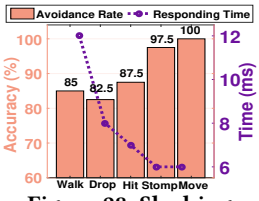

Figure 28: Sloshing interference avoidance rate and responding time.

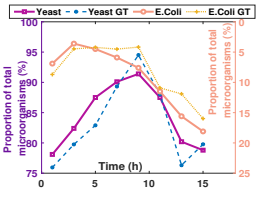

Figure 29: Microorganisms Composition.

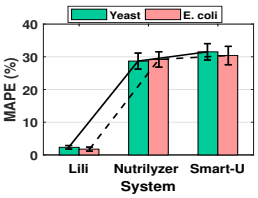

Figure 30: Concentration determination results of different systems.

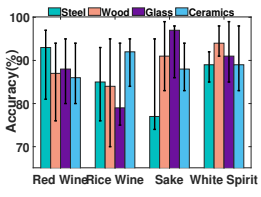

Figure 31: Alcohol concentration measurement accuracy.

6.3 Concentration Determination

6.3.1 Microorganism Composition. Different microorganisms have unique reflectance spectra. The amount of nutrients is limited in the aging process, creating competition between the yeast and other microorganisms. We clustered the absorption spectrum fingerprints using the K-means method, marking the proportions of yeast and *E. coli*. As shown in Figure 29, in liquor aged with *E. coli*, the MAPE in identifying the two microorganisms was only 2.33% and 1.77%. Note that because the liquid contained other interfering substances, the sum of the two microorganism contents was not 100% during the aging period.

We also wanted to see if there were sufficient advantages in monitoring microbial composition compared to the latest systems that use optical signals. We modified both Nutrilyzer [45] and Smart-U [19] to match our brewing vessel. Nutrilyzer [45] consisted of 16 LEDs in the ultraviolet, visible and near-infrared regions, and two piezoelectric sensors that were attached to the lid. Smart-U [19] consisted of 12 LEDs in the visible and near-infrared regions and a photodiode, which were also attached to the lid. Nutrilyzer [45] used a neural network with the top feature subset selected by correlation-based feature selection, while Smart-U [19] used Random Forest as the prediction algorithm. Lili utilized self-designed dimension expansion algorithm and K-means method. As shown in the Figure 30, Lili has the lowest MAPE, indicating that Lili's dimension expansion technology has exceptional capability for fine-grained monitoring.

6.3.2 Alcohol Concentration. Alcohol is produced by yeast fermentation, so the number of and changes in yeast can reflect the alcohol concentration. We used the yeast content results in Section 6.3.1 to calculate yeast accumulation from the beginning of aging to the moment of sampling. Then, we used the cumulative value, liquid volume and measurement vector $\vec{L}_{Mea}(t)$ as training parameters for the K-means method to determine the alcohol concentration. As shown in Figure 31, the alcohol content identification accuracy of the four wines during the brewing process was 88.13% on average (88.54%, 85.03%, 88.25% and 90.74%).

7 RELATED WORK

In this section, we review the related literature of Lili.

Liquid quality inspection. The conventional method of liquid quality inspection is based on the microorganisms counting method. The plate counting method [2] and ATP fluorescent microorganism detection method are the most common methods [3] applying in the liquid industry. However, they require complicated operating procedures and long-term microbial cultivation. Quality inspecting in fast and effective means is to measure the surface tension [24, 25] and absorption spectrum [20] based on the microorganism and its metabolism effect. Using the principle that the liquid's deterioration will produce different odours, the electronic nose [18] applies the odour fingerprint for inspection. However, these devices could introduce non-trivial deployment and maintenance cost. The latest working pH meter [16] uses the acid-base change of the liquid to identify whether it has deteriorated. However, its resolution is coarse-grained.

Liquid identification. There are many research achievements on liquids identification. Surface tension [26–28], absorption spectrum [29–31] and viscosity [46–48] are critical properties using for the fine-grained liquid components identification. They can be used to identify pollutants [49], determine blood cholesterol levels [50] and distinguish kidney diseases [23]. The latest research, Nutrilyzer [45] and Smart-U [19], apply the absorption spectrum and the photoacoustic effect to realize liquid identification. Al-light [51] proposes a smart ice cube device equipped with near-infrared and visible LEDs, which can estimate the alcohol concentration level. However, they are all limited by the narrowband spectrum of LEDs, making it challenging to achieve fine-grained liquid components identification, such as microorganisms changes. Liquids can also affect electromagnetic signals. TagScan [21] and RFIQ [52] pay attention to the RFID signal to determine the liquid composition. LiquID [22]

uses two independent ultra-wideband (UWB) units to judge the liquid by its dielectric constant. Mm-Humidity [53] uses millimeter waves to measure the liquid content in the air. The special devices or containers they use are still expensive. As a universal device, mobile phones can also identify liquids and achieve fine-grained measurements, such as surface tension [32, 33]. andThe latest technology is Vi-Liquid [23], which uses mobile phones to identify liquids through fine-grained viscosity differences. However, these solutions are not practical to apply to the brewing industry because they need high energy consumption and computation costs that lead to rugged use in long-term monitoring.

Light perception. As electromagnetic waves, optical signals are the common signal for perception. The object's absorption spectrum's uniqueness can be used for quality assessment [54] and food analysis [55] in the food industry. The transmission of light in different media will suffer the loss of perspective and scattering, and the measurement [56] of blood oxygen concentration uses this principle. The devices which generate unique light signals can be used to achieve precise indoor localization [57, 58]. Scattered light can also be used as a sensing signal, such as sensing gestures [59]. **Vibration perception.** Sensing technology using vibration signals has been booming in recent years, ranging from keystroke recognition [60, 61], user authentication [62–64]. Because the miniaturization and performance improvement of vibration motors and IMUs make more portable devices able to embed them. Oinput [61] and VibID [64] leverage passive and active vibration for identification, respectively. TouchPass[63] builds a behavior-irrelevant on-touch user authentication system on smartphones. The difference is that Lili uses a system composed of LEDs and PDs, which can feedback the impact of subtle microbial changes on the liquid.

8 CONCLUSION AND FUTURE WORK

In this article, we present a liquor quality monitor Lili. A Characteristic Offset Degree Measurement model is proposed to guide the photodiode to robustly and accurately calculate the surface tension under the low signal-to-noise ratio condition. Besides, the Dimension Expansion of Coarse-grained Absorption Spectrum model is also presented to solve the subtle changes in substances that monochromatic LEDs cannot detect. The error of surface tension and absorption spectrum measurement can reach 0.89 mN/m and 2.4% (MAPE). Through the measured value, 97.5% of the hazardous-health liquors can be identified. When aging wine, it can also identify the proportion of microorganisms and alcohol concentration. However, as a proof-of-concept prototype for liquor quality measurement, Lili still has some limitations to be addressed in our future work:

Liquid types: We plan to migrate to more practical liquid quality monitoring scenarios, including yoghurt brewing, pickle pickling. How to solve the problem of measuring the deterioration of different liquids is a significant problem that needs to be issued.

Types of containers: There are many extended application scenarios for liquid quality monitoring. However, these application scenarios use different containers, such as cans and cartons. Migrate different solution for the pervasive devices in different containers. It is also essential to adjust the device and size. We will address these problems in the future.

ACKNOWLEDGMENTS

This research was supported in part by the China NSFC Grant (U2001207, 61872248), Guangdong NSF 2017A030312008, Shenzhen Science and Technology Foundation (No. ZDSYS20190902092853047, R2020A045), the Project of DEGP (No.2019KCXTD005), the Guangdong "Pearl River Talent Recruitment Program" under the Grant 2019ZT08X603, Guangdong Science and Technology Foundation (2019B111103001, 2019B020209001), the China NSFC 61872246, Guangdong Special Support Program. Kaishun Wu is the corresponding author.

REFERENCES

[1] I. O. o. V. Organization, *International code of oenological practices 2020.* International Organisation of Vine and Wine (OIV), 2020. [Online]. Available: http://www.oiv.int/public/medias/7213/oiv-international-code-of-oenological-practices-2020-en.pdf

[2] B. Herigstad, M. Hamilton, and J. Heersink, "How to optimize the drop plate method for enumerating bacteria," *Journal of microbiological methods*, vol. 44, no. 2, pp. 121–129, 2001.

[3] K. Sakamoto, A. Margolles, H. W. Van Veen, and W. N. Konings, "Hop resistance in the beer spoilage bacterium Lactobacillus brevis is mediated by the ATP-binding cassette multidrug transporter HorA," *Journal of bacteriology*, vol. 183, no. 18, pp. 5371–5375, 2001.

[4] P. R. Grbin and P. A. HENSCHKE, "Mousy off-flavour production in grape juice and wine by dekkera and brettanomyces yeasts," *Australian Journal of Grape and Wine Research*, vol. 6, no. 3, pp. 255–262, 2000.

[5] H. Piao, E. Hawley, S. Kopf, R. DeScenzo, S. Sealock, T. Henick-Kling, and M. Hess, "Insights into the bacterial community and its temporal succession during the fermentation of wine grapes," *Frontiers in microbiology*, vol. 6, p. 809, 2015.

[6] F. Käferstein and M. Abdussalam, "Food safety in the 21st century." *Bulletin of the World Health Organization*, vol. 77, no. 4, p. 347, 1999.

[7] P. S. Mead, L. Slutsker, V. Dietz, L. F. McCaig, J. S. Bresee, C. Shapiro, P. M. Griffin, and R. V. Tauxe, "Food-related illness and death in the United States." *Emerging infectious diseases*, vol. 5, no. 5, p. 607, 1999.

[8] S. Hoffmann and E. Scallan, "Epidemiology, cost, and risk analysis of foodborne disease," in *Foodborne Diseases.* Elsevier, 2017, pp. 31–63.

[9] A. B. Snyder and R. W. Worobo, "The incidence and impact of microbial spoilage in the production of fruit and vegetable juices as reported by juice manufacturers," *Food Control*, vol. 85, pp. 144–150, 2018.

[10] V. Loureiro and M. Malfeito-Ferreira, "Spoilage activities of Dekkera/Brettanomyces spp," *Food spoilage microorganisms*, pp. 354–398, 2006.

[11] V. Fusco, D. Chieffi, F. Fanelli, A. F. Logrieco, G.-S. Cho, J. Kabisch, C. Böhnlein, and C. M. A. P. Franz, "Microbial quality and safety of milk and milk products in the 21st century," *Comprehensive Reviews in Food Science and Food Safety*, vol. 19, no. 4, pp. 2013–2049, 2020.

[12] Z. Gizaw, "Public health risks related to food safety issues in the food market: a systematic literature review," *Environmental health and preventive medicine*, vol. 24, no. 1, pp. 1–21, 2019.

[13] Z. Xu, Y. Luo, Y. Mao, R. Peng, J. Chen, T. Soteyome, C. Bai, L. Chen, Y. Liang, J. Su, and Others, "Spoilage lactic acid bacteria in the brewing industry," *Journal of microbiology and biotechnology*, vol. 30, no. 7, pp. 955–961, 2020.

[14] J. H. J. H. in't Veld, "Microbial and biochemical spoilage of foods: an overview," *International journal of food microbiology*, vol. 33, no. 1, pp. 1–18, 1996.

[15] W. H. Organization and Others, *WHO estimates of the global burden of foodborne diseases: foodborne disease burden epidemiology reference group 2007-2015.* World Health Organization, 2015.

[16] P. M. Shaibani, H. Etayash, K. Jiang, A. Sohrabi, M. Hassanpourfard, S. Naicker, M. Sadrzadeh, and T. Thundat, "Portable nanofiber-light addressable potentiometric sensor for rapid Escherichia coli detection in orange juice," *ACS sensors*, vol. 3, no. 4, pp. 815–822, 2018.

[17] A. F. Cunha, A. D. Lage, M. M. e Araújo, C. F. Abreu, A. R. Tassinari, M. A. Ferraz, K. Davenport, and M. Cerqueira, "ATP-Bioluminescence as a method to evaluated microbiological quality of UHT milk," *Arquivo Brasileiro de Medicina Veterinária e Zootecnia*, vol. 66, no. 6, pp. 1909–1916, 2014.

[18] M. L. Rodr\'\iguez-Méndez, J. A. De Saja, R. González-Antón, C. Garc\'\ia-Hernández, C. Medina-Plaza, C. Garc\'\ia-Cabezón, and F. Mart\'\in-Pedrosa, "Electronic noses and tongues in wine industry," *Frontiers in bioengineering and biotechnology*, vol. 4, p. 81, 2016.

[19] Q. Huang, Z. Yang, and Q. Zhang, "Smart-U: Smart Utensils Know what You Eat," in *Proceedings - IEEE INFOCOM*, vol. 2018-April. IEEE, 2018, pp. 1439–1447.

[20] H. M. Al-Qadiri, M. Lin, M. A. Al-Holy, A. G. Cavinato, and B. A. Rasco, "Monitoring quality loss of pasteurized skim milk using visible and short wavelength

near-infrared spectroscopy and multivariate analysis," *Journal of dairy science*, vol. 91, no. 3, pp. 950–958, 2008.
[21] J. Wang, J. Xiong, X. Chen, H. Jiang, R. K. Balan, and D. Fang, "TagScan: Simultaneous target imaging and material identification with commodity RFID devices," in *Proceedings of the Annual International Conference on Mobile Computing and Networking, MOBICOM*, vol. Part F131210, 2017, pp. 288–300.
[22] A. Dhekne, M. Gowda, Y. Zhao, H. Hassanieh, and R. R. Choudhury, "LiquID: A wireless liquid identifier," in *MobiSys 2018 - Proceedings of the 16th ACM International Conference on Mobile Systems, Applications, and Services*, 2018, pp. 442–454.
[23] Y. Huang, K. Chen, Y. Huang, L. Wang, and K. Wu, "Vi-liquid: unknown liquid identification with your smartphone vibration." in *MobiCom*, 2021, pp. 174–187.
[24] D. K. Ayhan, A. Temiz, F. A. Sana, and M. Gümü\csderelio\uglu, "Surface properties and exopolysaccharide production of surface-associated microorganisms isolated from a dairy plant," *Annals of Microbiology*, vol. 69, no. 9, pp. 895–907, 2019.
[25] Z. J. Mai, F. Lin, and J. M. Fan, "Research of Monitoring Deterioration of Milk by Using Surface Tension Coefficient and Viscosity," in *Advanced Materials Research*, vol. 455. Trans Tech Publ, 2012, pp. 467–470.
[26] V. B. Fainerman, R. Miller, and P. Joos, "The measurement of dynamic surface tension by the maximum bubble pressure method," *Colloid and Polymer Science*, vol. 272, no. 6, pp. 731–739, 1994.
[27] W. D. Harkins and F. E. Brown, "The determination of surface tension (free surface energy), and the weight of falling drops: The surface tension of water and benzene by the capillary height method." *Journal of the American Chemical Society*, vol. 41, no. 4, pp. 499–524, 1919.
[28] C. E. Stauffer, "The measurement of surface tension by the pendant drop technique," *The journal of physical chemistry*, vol. 69, no. 6, pp. 1933–1938, 1965.
[29] E. J. Hart and J. W. Boag, "Absorption spectrum of the hydrated electron in water and in aqueous solutions," *Journal of the American Chemical Society*, vol. 84, no. 21, pp. 4090–4095, 1962.
[30] L. N. M. Duyens, "The flattering of the absorption spectrum of suspensions, as compared to that of solutions," *Biochimica et biophysica acta*, vol. 19, pp. 1–12, 1956.
[31] R. M. Pope and E. S. Fry, "Absorption spectrum (380–700 nm) of pure water. II. Integrating cavity measurements," *Applied optics*, vol. 36, no. 33, pp. 8710–8723, 1997.
[32] N.-A. Goy, Z. Denis, M. Lavaud, A. Grolleau, N. Dufour, A. Deblais, and U. Delabre, "Surface tension measurements with a smartphone," *The Physics Teacher*, vol. 55, no. 8, pp. 498–499, 2017.
[33] S. Yue and D. Katabi, "Liquid testing with your smartphone," in *MobiSys 2019 - Proceedings of the 17th Annual International Conference on Mobile Systems, Applications, and Services*, 2019, pp. 275–286.
[34] T. K. Barik, P. R. Chaudhuri, A. Roy, and S. Kar, "Probing liquid surface waves, liquid properties and liquid films with light diffraction," *Measurement Science and Technology*, vol. 17, no. 6, p. 1553, 2006.
[35] M. Wei, S. Huang, J. Wang, H. Li, H. Yang, and S. Wang, "The study of liquid surface waves with a smartphone camera and an image recognition algorithm," *European Journal of Physics*, vol. 36, no. 6, p. 65026, 2015.
[36] A. J. T. Van Loon, *Analytical atomic absorption spectroscopy: selected methods*. Elsevier, 2012.
[37] C. Little, D. Lock, J. Barnes, and R. Mitchell, "Microbiological quality of food in relation to hazard analysis systems and food hygiene training in uk catering and retail premises." *Communicable disease and public health*, vol. 6, no. 3, pp. 250–258, 2003.
[38] H. P. A. o. U. Organization, *Guidelines for Assessing the Microbiological Safety of Ready-to-Eat Foods Placed on the Market*. Health Protection Agency of UK, 2009. [Online]. Available: https://assets.publishing.service.gov.uk/government/uploads/system/uploads/attachment_data/file/363146/Guidelines_for_assessing_the_microbiological_safety_of_ready-to-eat_foods_on_the_market.pdf
[39] F. Edition, "Guidelines for drinking-water quality," *WHO chronicle*, vol. 38, no. 4, pp. 104–108, 2011.
[40] J. O. Lundberg, M. T. Gladwin, A. Ahluwalia, N. Benjamin, N. S. Bryan, A. Butler, P. Cabrales, A. Fago, M. Feelisch, P. C. Ford *et al.*, "Nitrate and nitrite in biology, nutrition and therapeutics," *Nature chemical biology*, vol. 5, no. 12, pp. 865–869, 2009.
[41] S. Clegg, F. Yu, L. Griffiths, and J. A. Cole, "The roles of the polytopic membrane proteins nark, naru and nirc in escherichia coli k-12: two nitrate and three nitrite transporters," *Molecular microbiology*, vol. 44, no. 1, pp. 143–155, 2002.
[42] H. Muhamadali, A. Subaihi, M. Mohammadtaheri, Y. Xu, D. I. Ellis, R. Ramanathan, V. Bansal, and R. Goodacre, "Rapid, accurate, and comparative differentiation of clinically and industrially relevant microorganisms via multiple vibrational spectroscopic fingerprinting," *Analyst*, vol. 141, no. 17, pp. 5127–5136, 2016.
[43] K. Wang, H. Pu, and D.-W. Sun, "Emerging spectroscopic and spectral imaging techniques for the rapid detection of microorganisms: An overview," *Comprehensive reviews in food science and food safety*, vol. 17, no. 2, pp. 256–273, 2018.
[44] Y. Ohno, "Spectral design considerations for white LED color rendering," *Optical Engineering*, vol. 44, no. 11, p. 111302, 2005.
[45] T. Rahman, A. T. Adams, P. Schein, A. Jain, D. Erickson, and T. Choudhury, "Nutrilyzer: A mobile system for characterizing liquid food with photoacoustic effect," in *Proceedings of the 14th ACM Conference on Embedded Networked Sensor Systems, SenSys 2016*, 2016, pp. 123–136.
[46] J. de Vicente, M. T. López-López, J. D. Durán, and F. González-Caballero, "Shear flow behavior of confined magnetorheological fluids at low magnetic field strengths," *Rheologica Acta*, vol. 44, no. 1, pp. 94–103, 2004.
[47] C. Blom and J. Mellema, "Torsion pendula with electromagnetic drive and detection system for measuring the complex shear modulus of liquids in the frequency range 80-2500 Hz," *Rheologica Acta*, vol. 23, no. 1, pp. 98–105, 1984.
[48] M. Gottlieb, "Zero-shear-rate viscosity measurements for polymer solutions by falling ball viscometry," *Journal of Non-Newtonian Fluid Mechanics*, vol. 6, no. 2, pp. 97–109, 1979.
[49] I. N. Aribudiman, "Seepage in soil from the difference of water viscosity using Geo-studio SEEP/W program," *International research journal of engineering, IT & scientific research*, vol. 5, no. 1, pp. 15–26, 2019.
[50] C. Tripolino, C. Irace, C. Carallo, F. B. Scavelli, and A. Gnasso, "Body fat and blood rheology: Evaluation of the association between different adiposity indices and blood viscosity," *Clinical Hemorheology and Microcirculation*, vol. 65, no. 3, pp. 241–248, 2017.
[51] H. Matsui, T. Hashizume, and K. Yatani, "Al-light: An Alcohol-Sensing Smart Ice Cube," *Proceedings of the ACM on Interactive, Mobile, Wearable and Ubiquitous Technologies*, vol. 2, no. 3, pp. 1–20, 2018.
[52] U. Ha, Y. Ma, Z. Zhong, T. M. Hsu, and F. Adib, "Learning food quality and safety from wireless stickers," in *HotNets 2018 - Proceedings of the 2018 ACM Workshop on Hot Topics in Networks*, 2018, pp. 106–112.
[53] Q. Dai, Y. Huang, L. Wang, R. Ruby, and K. Wu, "mm- humidity: Fine-grained humidity sensing with millimeter wave signals," in *2018 IEEE 24th International Conference on Parallel and Distributed Systems (ICPADS)*, 2018, pp. 204–211.
[54] N. Prieto, R. Roehe, P. Lav\'\in, G. Batten, and S. Andrés, "Application of near infrared reflectance spectroscopy to predict meat and meat products quality: A review," *Meat science*, vol. 83, no. 2, pp. 175–186, 2009.
[55] Y. Ozaki, W. F. McClure, and A. A. Christy, *Near-infrared spectroscopy in food science and technology*. John Wiley & Sons, 2006.
[56] F. Gao, Q. Peng, X. Feng, B. Gao, and Y. Zheng, "Single-wavelength blood oxygen saturation sensing with combined optical absorption and scattering," *IEEE Sensors Journal*, vol. 16, no. 7, pp. 1943–1948, 2015.
[57] C. Zhang and X. Zhang, "Pulsar: Towards ubiquitous visible light localization," in *Proceedings of the 23rd Annual International Conference on Mobile Computing and Networking*, 2017, pp. 208–221.
[58] ——, "LiTell: Robust indoor localization using unmodified light fixtures," in *Proceedings of the 22nd Annual International Conference on Mobile Computing and Networking*, 2016, pp. 230–242.
[59] R. H. Venkatnarayan and M. Shahzad, "Gesture recognition using ambient light," *Proceedings of the ACM on Interactive, Mobile, Wearable and Ubiquitous Technologies*, vol. 2, no. 1, pp. 1–28, 2018.
[60] J. Liu, Y. Chen, M. Gruteser, and Y. Wang, "VibSense: Sensing Touches on Ubiquitous Surfaces through Vibration," in *2017 14th Annual IEEE International Conference on Sensing, Communication, and Networking, SECON 2017*. IEEE, 2017, pp. 1–9.
[61] Y. Huang, S. Cai, L. Wang, and K. Wu, "Oinput: A Bone-Conductive QWERTY Keyboard Recognition for Wearable Device," in *Proceedings of the International Conference on Parallel and Distributed Systems - ICPADS*, vol. 2018-December. IEEE, 2019, pp. 946–953.
[62] S. Pan, T. Yu, M. Mirshekari, J. Fagert, A. Bonde, O. Mengshoel, H. Noh, and P. Zhang, "Footprintid: Indoor pedestrian identification through ambient structural vibration sensing," *Proceedings of the ACM on Interactive, Mobile, Wearable and Ubiquitous Technologies*, vol. 1, pp. 1–31, 09 2017.
[63] X. Xu, J. Yu, Y. chen, Q. Hua, Y. Zhu, Y.-C. Chen, and M. Li, "Touchpass: Towards behavior-irrelevant on-touch user authentication on smartphones leveraging vibrations," in *Proceedings of the 26th Annual International Conference on Mobile Computing and Networking*, ser. MobiCom '20. New York, NY, USA: Association for Computing Machinery, 2020. [Online]. Available: https://doi.org/10.1145/3372224.3380901
[64] L. Yang, W. Wang, and Q. Zhang, "VibID: User Identification through Bio-Vibrometry," in *2016 15th ACM/IEEE International Conference on Information Processing in Sensor Networks, IPSN 2016 - Proceedings*. IEEE, 2016, pp. 1–12.